Smart Structures and Systems, *Vol. 15, No. 5 (2015) 1271-1291*
DOI: http://dx.doi.org/10.12989/sss.2015.15.5.1271

Theoretical analysis of superelastic SMA helical structures subjected to axial and torsional loads

Xiang Zhou*[1] and Zhong You[2a]

[1]*School of Aeronautics and Astronautics, Shanghai Jiao Tong University, 800 Dongchuan Road, Shanghai, P.R. China*
[2]*Department of Engineering Science, University of Oxford, Parks Road, Oxford, UK*

(Received December 2, 2013, Revised April 24, 2014, Accepted May 5, 2014)

Abstract. Helical structures made of superelastic shape memory alloys are widely used as interventional medical devices and active actuators. These structures generally undergo large deformation during expansion or actuation. Currently their behaviour is modelled numerically using the finite element method or obtained through experiments. Analytical tools are absent. In this paper, an analytical approach has been developed for analyzing the mechanical responses of such structures subjected to axial and torsional loads. The simulation results given by the analytical approach have been compared with both numerical and experimental data. Good agreements between the results indicate that the analysis is valid.

Keywords: helical structure; shape memory alloy; superelastic; analytical model

1. Introduction

Helical steel structures have long been used to make springs and braded hose pipes. Analytical formulas exist to model their behaviour. More recently helical structures made of superelastic shape memory alloys (abbreviated to SMA) such as Nitinol, have been used as interventional medical stents (Roguin *et al.* 1999, Hill *et al.* 2004, Zhou *et al.* 2008) and actuator devices (Chaudhry and Rogers 1991, Degeratu 2008, Khan and Srinivasan 2011, Spinella and Dragoni 2010, von Riesen 2008, Yates and Kalamkarov 2013). These structures in general undergo large deformation. For example, a stent has to be folded to small volume for delivery and it expands once it is released from a delivery catheter. The current means to investigate the mechanical behaviours in the design of such structures are limited to the finite element analysis (abbreviated to FEA) or experiments. Although the FEA is a valuable tool, it has several drawbacks such as its solver-dependent nature, the complexity in creating the correct finite element model and the prolonged computational time. On the other hand, a well devised experiment can be expensive. Therefore, it is desirable to have an analytical method, as a complement to the FEA or experiments, which can accurately predict the behaviour of the SMA helical structures.

Theoretical solutions to a helical structure subjected to axial and torsional loads are available in

*Corresponding author, Associate Professor, E-mail: xiangzhou@sjtu.edu.cn
[a] Professor of Engineering Science, E-mail: zhong.you@eng.ox.ac.uk

http://www.techno-press.org/?journal=sss&subpage=8 ISSN: 1738-1584 (Print), 1738-1991 (Online)

literatures (Mansfield 1980). However, these theoretical solutions were developed for linear elastic material. For superelastic helical structure, the martensite formation can be initiated as loading is increased, which greatly increases the complexity of the problem. Therefore, those theoretical solutions based on a linear elastic material model are no longer applicable for superelastic SMA helical structures.

This paper presents attempts to develop an analytical approach for analysis of the mechanical responses of the superelastic SMA helical structures subject to axial and torsional loads. The layout of the paper is as follows. The basic assumptions made to the SMA material are discribed in Section 2. Section 3 derives the main theory constituting the analytical model. The simulation results are provided in Section 4. Finally, a summarization to the paper is given in Section 5.

2. Basic assumptions

The true material properties of a superelastic SMA, well-illustrated in the publications (Auricchio *et al.* 1997, Aurrichio and Sacco 1997, Boyd and Lagoudas 1996, Qidwai and Lagoudas 2000, Brocca *et al.* 2002, Peultier *et al.* 2006, Zhu and Zhang 2007, Arghavani *et al.* 2010, He and Sun 2011), are very complex. It is necessary to make certain degrees of simplification to the material model in order to derive an analytical solution for the present problem. Here, three assumptions are made to the material model.

First, it is assumed that the superelastic normal and shear deformation behaviours are independent of each other (Toi *et al.* 2004), meaning that the shear stress-strain relationship of the material is not affected by the normal loading, or vice versa.

Second, it is assumed that the shear stress-strain relationship of a superelastic SMA is qualitatively similar to the normal stress-strain relationship (Toi *et al.* 2004). Therefore, material constants of the shear stress-strain relationship can be determined by the normal results obtained from a uniaxial tensile test, as shown in Table 1, in which μ is the poisson's ratio and ζ is a coefficient.

Table 1 Material constants of normal and shear stress-strain relationships

Normal	Shear	Description
E_A	$G_A = E_A/2(1+\mu)$	Elastic and shear modulus of Austenite
E_M	$G_M = E_M/2(1+\mu)$	Elastic and shear modulus of Martensite
σ_M^s	$\tau_M^s = \sigma_M^s/\zeta$	Starting transformation stress of loading
σ_M^f	$\tau_M^f = \sigma_M^f/\zeta$	End transformation stress of loading
σ_A^s	$\tau_A^s = \sigma_A^s/\zeta$	Starting transformation stress of unloading
σ_A^f	$\tau_A^f = \sigma_A^f/\zeta$	End transformation stress of unloading
ε_L	$\gamma_L = \varepsilon_L$	Maximum residual strain

The third assumption regards a simplified constitutive law for the superelastic behaviour of SMA. Although various constitutive models of the superelastic behavior of SMA have been proposed in literatures (Auricchio *et al.* 1997, Aurrichio and Sacco 1997, Boyd and Lagoudas 1996, Qidwai and Lagoudas 2000) based on theories of thermodynamics or general plasticity, these material constitutive laws are too complex to be implemented analytically. Atanackovic and Achenbach and Achenbach (1989) derived the moment-curvature relation for a superelastic SMA beam subject to pure bending. In their model, it has been assumed that $E_A = E_M$, $\sigma_M^s = \sigma_M^f$ and $\sigma_A^s = \sigma_A^f$ for the material, leading to that the loading-unloading paths of the fully austenite phase and the fully martensite phase are parallel on the stress-strain graph, and so are the loading and unloading plateaus. Furthermore, it has been assumed that if the unloading started from a point on the loading plateau, it proceeds along a line parallel to the loading-unloading path of the fully austenite phase.

This paper adopts a simplified constitutive law for the superelastic SMA so that a theoretical model for the problem under consideration can be derived. It is similar to that given in (Achenbach and Achenbach 1989) except that the differences between $E_A$andE_M, σ_M^sandσ_M^f, and σ_A^s and σ_A^f are taken into account. The martensite volume fraction ξ is assumed to be proportional to the stress σ during loading plateau, given by

$$\xi = \frac{\sigma - \sigma_M^s}{\sigma_M^f - \sigma_M^s} \tag{1}$$

and the Young's modulus of the material is taken as a function of the martensite volume fraction ξ, given by

$$E_\xi = E_A + \xi(E_M - E_A) \tag{2}$$

The normal stress-strain relationship for a SMA in the superelastic range is given in Fig. 1, where ε_M^s, ε_M^f, ε_A^s and $\varepsilon_A^f$are respectively the starting transformation strain of loading, the end transformation strain of loading, the starting transformation strain of unloading, and the end transformation strain of unloading, given by

$$\varepsilon_M^s = \frac{\sigma_M^s}{E_A}, \varepsilon_M^f = \frac{\sigma_M^f}{E_M} + \varepsilon_L \tag{3}$$

$$\varepsilon_A^s = \frac{\sigma_A^s}{E_M} + \varepsilon_L, \varepsilon_A^f = \frac{\sigma_A^f}{E_A} \tag{4}$$

and E_L and $E_U$are respectively the slopes of loading and unloading plateaus, given by

$$E_L = \frac{\sigma_M^f - \sigma_M^s}{\varepsilon_M^f - \varepsilon_M^s} \tag{5}$$

$$E_U = \frac{\sigma_A^f - \sigma_A^s}{\varepsilon_A^f - \varepsilon_A^s} \tag{6}$$

According to the second assumption, the martensite fraction ξ_τ due to shear loading and shear modulus G can be written as

$$\xi_\tau = \frac{\tau - \tau_M^s}{\tau_M^f - \tau_M^s} \tag{7}$$

and

$$G_{\xi_\tau} = G_A + \xi_\tau (G_M - G_A) \tag{8}$$

3. Analysis

3.1 Beam subjected to pure bending

Consider now a straight beam subjected to a bending moment *M*, as shown in Fig. 2, where the dash-dotted line represents the neutral surface and *t* is the thickness of the beam. Strain ε in a layer whose distance is *y* from the neutral surface is given by

$$\varepsilon = ky \tag{9}$$

where k is the curvature of the beam at a certain moment. According to Eq. (9), the further a layer is away from the neutral surface, the larger the strain in the layer is, and the maximum strain in the beam occurs at the outmost surface of the beam, given by

$$\varepsilon_{max} = k\frac{t}{2} \tag{10}$$

If ε_{max} is smaller than ε_M^S, i.e.

$$\varepsilon_{max} = k\frac{t}{2} < \varepsilon_M^S \Rightarrow k < \frac{2\varepsilon_M^S}{t} \tag{11}$$

the entire beam throughout the section remains elastic. In this case, the stress distribution across the beam, which is a function of both k and y, is given by

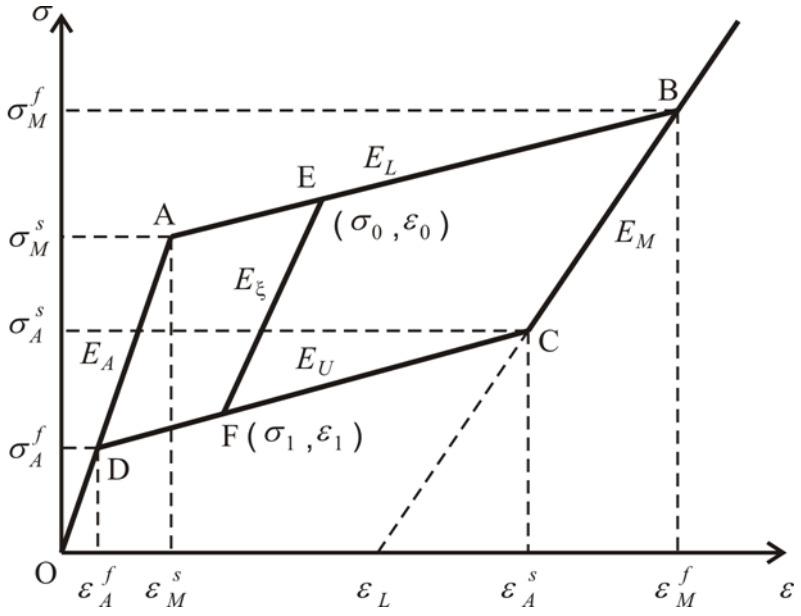

Fig. 1 Normal stress-strain diagram of superelastic SMA

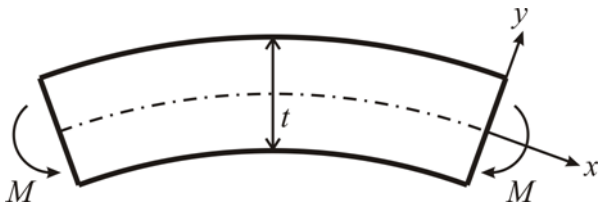

Fig. 2 A beam subjected to bending

$$\sigma(k,y) = E_A\varepsilon = E_A ky \tag{12}$$

If k becomes greater than $2\varepsilon_M^S/t$, the outmost layer of the beam will first reach point A in Fig. 1 and the beam is consequently divided into a transformation region and an elastic core of fully austenite. As the beam is further bent, the transformation region develops towards the neutral surface and the elastic core of fully austenite becomes smaller. On the outer border y_e of the elastic core, the strain equals the starting transformation strain of loading ε_M^S. Therefore, y_e can be found by

$$\varepsilon(y_e) = ky_e = \varepsilon_M^S \Rightarrow y_e = \frac{\varepsilon_M^S}{k} \tag{13}$$

The stress distribution within the elastic core, i.e., $y < y_e$, is the same as Eq. (12). An arbitrary point in the transformation region, i.e., $y > y_e$, proceeds along line AB in Fig. 1. Therefore, the stress distribution outside the elastic core is given by

$$\sigma(k,y) = \sigma_M^S + E_L(\varepsilon - \varepsilon_M^S) = \sigma_M^S + E_L(ky - \varepsilon_M^S) \tag{14}$$

Eq. (14) remains valid until the outmost layer reaches point B in Fig. 1. In this situation, the maximum strain equals the end transformation strain of loading $\varepsilon_M^f$and the critical curvature can be found by

$$\varepsilon_{max} = k\frac{t}{2} = \varepsilon_M^f \Rightarrow k = \frac{2\varepsilon_M^f}{t} \tag{15}$$

When $k > 2\varepsilon_M^f$, the beam is divided into three distinct regions, i.e., an elastic core of fully austenite – region I, a transformation middle region – region II, and a fully martensite outer region – Region III. The border between regions I and II is given by Eq. (13). The strain equals the end transformation strain of loading ε_M^fat the border between regions II and III. Therefore, there is

$$\varepsilon(y_t) = ky_t = \varepsilon_M^f \Rightarrow y_t = \frac{\varepsilon_M^f}{k} \tag{16}$$

In the elastic core, the stress distribution is again the same as Eq. (12). In the transformation region, the stress distribution is the same as Eq. (14). A point in region III proceeds along line CB in Fig. 1. Therefore, the stress distribution in this region is given by

$$\sigma(k,y) = E_M(\varepsilon - \varepsilon_L) = E_M(ky - \varepsilon_L) \tag{17}$$

In summary, the stress distribution across the beam during bending can be written as

$$\sigma(k,y) = E_A ky;\ when\ k \le \frac{2\varepsilon_M^S}{t} \tag{18}$$

$$\sigma(k,y) = \begin{cases} E_A ky, 0 < y \le \frac{\varepsilon_M^S}{k} \\ \sigma_M^S + E_L(ky - \varepsilon_M^S), \frac{\varepsilon_M^S}{k} < y \le \frac{t}{2} \end{cases};\ when\ \frac{2\varepsilon_M^S}{t} < k \le \frac{2\varepsilon_M^f}{t} \tag{19}$$

$$\sigma(k,y) = \begin{cases} E_A ky, 0 < y \le \frac{\varepsilon_M^S}{k} \\ \sigma_M^S + E_L(ky - \varepsilon_M^S), \frac{\varepsilon_M^S}{k} < y \le \frac{\varepsilon_M^f}{k}; when\ k > \frac{2\varepsilon_M^f}{t} \\ E_M(ky - \varepsilon_L), \frac{\varepsilon_M^f}{k} < y \le \frac{t}{2} \end{cases} \tag{20}$$

Consider now unbending of the beam after it is bent. In this case, the curvature of the beam at the end of bending has to be taken into account because this curvature acts as the initial curvature of the unbending process. Denote $k_0$as the initial curvature of unbending in subsequent discussion. The stress distribution across the beam during unbending will be a function of *k*, *y* and k_0.

First, consider the case when $k_0 < 2\varepsilon_M^S/t$. In this case, the entire beam is elastic at the beginning of unbending. As *k* decreases, the stress-strain relationship of any point in the beam proceeds along AO in Fig. 1. Therefore, the stress distribution in the whole cross section of the beam is given by

$$\sigma(k,y;k_0) = E_A ky \tag{21}$$

When $2\varepsilon_M^S/t < k_0 < 2\varepsilon_M^f/t$, the beam is initially divided into two regions i.e., an elastic core and a transformation region at the beginning of unbending. The border between the two regions is given by$y = \varepsilon_M^S/k_0$, according to Eq. (13). In the elastic core, i.e., $y < \varepsilon_M^S/k_0$, the stress distribution is the same as Eq. (21). The attention is focused on the stress distribution in the transformation region, i.e., $y > \varepsilon_M^S/k_0$. Consider an arbitrary point in the transformation region. At the beginning of unbending, this point is on line AB in Fig. 1, denoted by point E. The initial strain ε_0 of this point is $k_0 y$, and the initial stress σ_0 is given by

$$\sigma_0 = \sigma_M^S + E_L(k_0 y - \varepsilon_M^S) \tag{22}$$

As *k* decreases, the stress-strain relationship of this point proceeds along a path following lines EF, FD and finally DO in Fig. 1. During the course, there are two critical values for *k* occurring at points F and D, respectively. To find out the two critical values for *k*, the strains at points F and D have to be obtained first. Considering both Eqs. (1) and (22), the martensite fraction ξat point E becomes

$$\xi = \frac{\sigma_0 - \sigma_M^S}{\sigma_M^f - \sigma_M^S} = \frac{E_L(k_0 y - \varepsilon_M^S)}{\sigma_M^f - \sigma_M^S} \tag{23}$$

Substituting Eq. (23) into Eq. (2), Young's ModulusE_y, which is the slope of line EF, can be found as

$$E_y = E_A + \frac{E_L(k_0 y - \varepsilon_M^S)}{\sigma_M^f - \sigma_M^S}(E_M - E_A) \tag{24}$$

Through Eq. (24), the stress $\sigma_1$and strainε_1 at point F can be related to the stress and strain at point E by

$$\frac{\sigma_1-\sigma_0}{\varepsilon_1-\varepsilon_0}=E_y \tag{25}$$

In addition, note that point F is on line DC. Therefore, the stress and strain at point F have to satisfy

$$\sigma_1=\sigma_A^f+E_U(\varepsilon_1-\varepsilon_A^f) \tag{26}$$

By solving Eqs. (25) and (26) together and considering Eq. (22), the strain $\varepsilon_1$at point F can be written as

$$\varepsilon_1=\frac{\sigma_M^s-\sigma_A^f-E_L\varepsilon_M^s+E_U\varepsilon_A^f+(E_L-E_y)k_0y}{E_U-E_y} \tag{27}$$

Using Eq. (9), the critical value for *k* at point F can be found as

$$k_1^{cr}=\frac{\varepsilon_1}{y}=\frac{\sigma_M^s-\sigma_A^f-E_L\varepsilon_M^s+E_U\varepsilon_A^f+(E_L-E_y)k_0y}{(E_U-E_y)y} \tag{28}$$

The strain at point D is the end transformation strain of unloading ε_A^f. Therefore, the critical value for *k* at point D is

$$k_2^{cr}=\frac{\varepsilon_A^f}{y} \tag{29}$$

With the two critical values for *k* having been found, the rest work to find the stress distribution is trivial. When *k* is smaller than $k_0$but larger than k_1^{cr}, the stress-strain relationship of any point in the transformation region proceeds along line EF, and the stress distribution becomes

$$\sigma(k,y;k_0)=\sigma_M^s-E_L\varepsilon_M^s+\left(E_L-E_y\right)k_0y+E_yky \tag{30}$$

When *k* is smaller than k_1^{cr} but larger than k_2^{cr}, the stress-strain relationship of any point in the transformation region proceeds along line FD, and the stress distribution is

$$\sigma(k,y;k_0)=\sigma_A^f+E_U(ky-\varepsilon_A^f) \tag{31}$$

When *k* becomes smaller than k_2^{cr}, the stress-strain relationship of any point in the transformation region proceeds along line DO, and the stress distribution is

$$\sigma(k,y;k_0)=E_Aky \tag{32}$$

Finally, consider the case when $2\varepsilon_M^f/t<k_0$. In this case, the beam is divided into three regions at the beginning of unbending, i.e., a fully austenite elastic core, a transformation region and a fully martensite outer region. According to Eq. (20), the border between the elastic core and the transformation region is given by $y_e=\varepsilon_M^s/k_0$. The border between the transformation region and the fully martensite region is given by$y_t=\varepsilon_M^f/k_0$. In the elastic core, the stress distribution is the same as Eq. (21). In the transformation region, the stress distribution follows Eqs. (30)-(32) as *k* decreases. For an arbitrary point in the fully martensite region, its stress-strain relationship proceeds along a path following lines BC, CD and finally DO in Fig. 1. The critical values for *k* occurs at points C and D. Eq. (29) has given the critical value for *k* at point D. At point C, the

strain equals the starting transformation strain of unloading ε_A^s. Therefore the critical value for k at point C is

$$k_3^{cr} = \frac{\varepsilon_A^s}{y} \tag{33}$$

When k is smaller than $k_0$but larger than k_3^{cr}, the stress-strain relationship of a point in the fully martensite region proceeds along line BC and the stress distribution is

$$\sigma(k, y; k_0) = E_M(ky - \varepsilon_L) \tag{34}$$

When k is smaller than k_3^{cr} but larger thank_2^{cr}, the stress distribution in the fully martensite region is the same as Eq. (31). When k is smaller thank_2^{cr}, the stress distribution is the same as Eq. (32).

In summary, the stress distribution across the beam during unbending is given by

$$\sigma(k, y; k_0) = E_A ky, k < k_0;\ when\ k_0 < \frac{2\varepsilon_M^s}{t} \tag{35}$$

$$\sigma(k, y; k_0) = \begin{cases} E_A ky, if\ k < k_0 \,\&\, y < \frac{\varepsilon_M^s}{k_0} \parallel k < k_2^{cr} \,\&\, y > \frac{\varepsilon_M^s}{k_0} \\ \sigma_M^s - E_L\varepsilon_M^s + \left(E_L - E_y\right)k_0 y + E_y ky, if\ k_1^{cr} < k < k_0 \,\&\, y > \frac{\varepsilon_M^s}{k_0}; \\ \sigma_A^f + E_U\left(ky - \varepsilon_A^f\right), if\ k_2^{cr} < k < k_1^{cr} \,\&\, y > \frac{\varepsilon_M^s}{k_0} \end{cases} \tag{36}$$

$$; when\ \frac{2\varepsilon_M^s}{t} < k_0 < \frac{2\varepsilon_M^f}{t}$$

$$\sigma(k, y; k_0) = \begin{cases} E_A ky, if\ k < k_0 \,\&\, y < \frac{\varepsilon_M^s}{k_0} \parallel k < k_2^{cr} \,\&\, \frac{\varepsilon_M^s}{k_0} < y < \frac{\varepsilon_M^f}{k_0} \parallel k < k_2^{cr} \,\&\, \frac{\varepsilon_M^f}{k_0} < y \\ \sigma_M^s - E_L\varepsilon_M^s + \left(E_L - E_y\right)k_0 y + E_y ky, if\ k_1^{cr} < k < k_0 \,\&\, \frac{\varepsilon_M^s}{k_0} < y < \frac{\varepsilon_M^f}{k_0} \\ \sigma_A^f + E_U\left(ky - \varepsilon_A^f\right), if\ k_2^{cr} < k < k_1^{cr} \,\&\, \frac{\varepsilon_M^s}{k_0} < y < \frac{\varepsilon_M^f}{k_0} \parallel k_2^{cr} < k < k_3^{cr} \,\&\, y > \frac{\varepsilon_M^f}{k_0} \\ E_M(ky - \varepsilon_L), if\ k_3^{cr} < k < k_0 \,\&\, y > \frac{\varepsilon_M^f}{k_0} \end{cases}$$

$$; when\ k_0 > \frac{2\varepsilon_M^f}{t} \tag{37}$$

where $\parallel$ and & are "or" and "and" operations, respectively.

Using the stress distribution across the beam discussed above, it is easy to get the bending moment. For a beam with a rectangular cross-section, the bending moment as a function of the curvature k is given by

$$M(k) = 2b\int_0^{t/2} \sigma(k, y) y dy \tag{38}$$

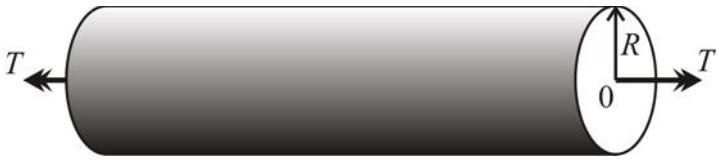

Fig. 3 A beam subjected to torsion

where b is the width of the beam. In Eq. (38), it is assumed that the stress distribution of the region in compression is the same as that of the region in tension but has the opposite sign. However, it is not difficult to take the differences of stress between compression and tension into account based on the discussion above to derive the stress distribution in compression separately. In this case, Eq. (38) needs to be modified to

$$M(k) = b\int_0^{t/2}\sigma_t(k,y)ydy + b\int_{-t/2}^{0}\sigma_c(k,y)ydy \tag{39}$$

where $\sigma_t(k,y)$ is the stress distribution in tension and $\sigma_c(k,y)$ is the stress distribution in compression. For a beam with a circular cross-section, the bending moment is given by

$$M(k) = 4\int_0^{R}\sigma(k,y)y\sqrt{r^2-y^2}dy \tag{40}$$

where r is the radius of the cross-section.

3.2 Beam subjected to pure torsion

In this section, a straight beam subjected to a torque T is considered, as shown in Fig. 3. Because it is assumed in section 2 that the shear stress-strain relationship is similar to the normal stress-strain relationship, the derivation of stress distribution across a beam subjected to torsion will therefore be similar to the derivation given in section 3.1. One major difference between bending and torsion is the relationship between the strain and the deformation. In bending, the normal strain is related to the curvature of the beam through Eq. (9). In torsion, the shear strain γ in a circular cross-section is related to the twist of the beam k_{xy}via

$$\gamma = rk_{xy} \tag{41}$$

where r is the radius of the layer at which the shear strain is calculated. Note that the form of Eq. (41) is similar to that of Eq. (9). Therefore, the stress distribution across the beam in torsion should have a similar form as that of bending. The detailed derivation for torsion is not provided for simplicity. The results are directly given below.

For torsional loading,

$$\tau\left(k_{xy},r\right) = G_A k_{xy} r;\ when\ k_{xy} \le \frac{\gamma_M^s}{R} \tag{42}$$

$$\tau\left(k_{xy},r\right) = \begin{cases} G_A k_{xy} r, 0 < r \le \frac{\gamma_M^s}{k_{xy}} \\ \tau_M^s + G_L\left(k_{xy}r - \gamma_M^s\right), \frac{\gamma_M^s}{k_{xy}} < r \le R \end{cases};\ when\ \frac{\gamma_M^s}{R} < k_{xy} \le \frac{\gamma_M^f}{R} \tag{43}$$

$$\tau(k_{xy},r)=\begin{cases} G_A k_{xy} r, 0<r\le \frac{\gamma_M^s}{k_{xy}} \\ \tau_M^s+G_L\left(k_{xy}r-\gamma_M^s\right), \frac{\gamma_M^s}{k_{xy}}<r\le \frac{\gamma_M^f}{k_{xy}};\ when\ k_{xy}>\frac{\gamma_M^f}{R} \\ G_M\left(k_{xy}r-\gamma_L\right), \frac{\gamma_M^f}{k_{xy}}<r\le R \end{cases} \tag{44}$$

For torsional unloading

$$\tau(k_{xy},r;k_{xy0})=G_A k_{xy} r, k_{xy}<k_{xy0};\ when\ k_{xy0}<\frac{\gamma_M^s}{R} \tag{45}$$

$$\tau(k_{xy},r;k_{xy0})=\begin{cases} G_A k_{xy} r, if\ k_{xy}<k_{xy0}\ \&\ r<\frac{\gamma_M^s}{k_{xy0}}\ \|\ k_{xy}<k_{xy2}^{cr}\ \&\ r>\frac{\gamma_M^s}{k_{xy0}} \\ \tau_M^s-G_L\gamma_M^s+\left(G_L-G_y\right)k_{xy0}r+G_y k_{xy} r, if\ k_{xy1}^{cr}<k_{xy}<k_{xy0}\ \&\ r>\frac{\gamma_M^s}{k_{xy0}} \\ \tau_A^f+G_U\left(k_{xy}r-\gamma_A^f\right), if\ k_{xy2}^{cr}<k_{xy}<k_{xy1}^{cr}\ \&\ r>\frac{\gamma_M^s}{k_{xy0}} \end{cases}$$

$$;\ when\ \frac{\gamma_M^s}{R}<k_{xy0}<\frac{\gamma_M^f}{R} \tag{46}$$

$$\tau(k_{xy},r;k_{xy0})$$

$$=\begin{cases} G_A k_{xy} r, if\ k_{xy}<k_{xy0}\ \&\ r<\frac{\gamma_M^s}{k_{xy0}}\ \|\ k_{xy}<k_{xy2}^{cr}\ \&\ \frac{\gamma_M^s}{k_{xy0}}<r<\frac{\gamma_M^f}{k_{xy0}} \\ \|\ k_{xy}<k_{xy2}^{cr}\ \&\ r>\frac{\gamma_M^f}{k_{xy0}} \\ \tau_M^s-G_L\gamma_M^s+\left(G_L-G_y\right)k_{xy0}r+G_y k_{xy} r, if\ k_{xy1}^{cr}<k_{xy}<k_{xy0}\ \&\ \frac{\gamma_M^s}{k_{xy0}}<r<\frac{\gamma_M^f}{k_{xy0}} \\ \tau_A^f+G_U\left(k_{xy}r-\gamma_A^f\right), if\ k_{xy2}^{cr}<k_{xy}<k_{xy1}^{cr}\ \&\ \frac{\gamma_M^s}{k_{xy0}}<r<\frac{\gamma_M^f}{k_{xy0}} \\ \|\ k_{xy2}^{cr}<k_{xy}<k_{xy3}^{cr}\ \&\ r>\frac{\gamma_M^f}{k_{xy0}} \\ G_M\left(k_{xy}r-\gamma_L\right), if\ k_{xy3}^{cr}<k_{xy}<k_{xy0}\ \&\ r>\frac{\gamma_M^f}{k_{xy0}} \end{cases}$$

$$;\ when\ k_{xy0}>\frac{\gamma_M^f}{R} \tag{47}$$

where ‖ and & are "or" and "and" operations, respectively, and

$$\gamma_M^s=\frac{\tau_M^s}{G_A}, \gamma_M^f=\frac{\tau_M^f}{G_M}+\gamma_L \tag{48}$$

$$\gamma_A^s=\frac{\tau_A^s}{G_M}+\gamma_L, \gamma_A^f=\frac{\tau_A^f}{G_A} \tag{49}$$

$$G_L = \frac{\tau_M^f - \tau_M^s}{\gamma_M^f - \gamma_M^s} \tag{50}$$

$$G_U = \frac{\tau_A^f - \tau_A^s}{\gamma_A^f - \gamma_A^s} \tag{51}$$

$$G_y = G_A + \frac{\tau_M^s + G_L(k_{xy0}r - \gamma_M^s)}{\tau_M^f - \tau_M^s}(G_M - G_A) \tag{52}$$

$$k_{xy1}^{cr} = \frac{\tau_M^s - \tau_A^f - G_L\gamma_M^s + G_U\gamma_A^f + (G_L - G_y)k_{xy0}r}{(G_U - G_y)r} \tag{53}$$

$$k_{xy2}^{cr} = \frac{\gamma_A^f}{r} \tag{54}$$

and

$$k_{xy3}^{cr} = \frac{\gamma_A^s}{r} \tag{55}$$

Finally, the torque *T* applied to the beam as a function of the twist k_{xy} is given by

$$T(k_{xy}) = 2\pi \int_0^R \tau(k_{xy}, r) r^2 dr \tag{56}$$

Incidentally, here only the torque *T* of a beam with a circular cross section is given in detail because Eq. (41) stands exactly for this type of beam. For a beam with a rectangular cross section, there is no exact relationship between the shear strain γ and the twist k_{xy}. Nevertheless, anapproximate solution can still be obtained by using the methodology provided above assuming (Young 1989)

$$\gamma \approx 2yk_{xy} \tag{57}$$

And torque *T* is therefore given by

$$T(k_{xy}) = 2b \int_0^{t/2} \tau(k_{xy}, y) y dy \tag{58}$$

where *b* and *t* are the width and thickness of the beam.

3.3 Helical structure subjected to axial load and torsion

Consider now a helical structure subjected to an axial load *P* and a torque *T*, as shown in Fig. 4. Bending moment $M_b$and torque $M_t$on an arbitrary cross section of the helix coil are (Timoshenko 1956)

$$M_b = T\cos\alpha_H - PR_H\sin\alpha_H \tag{59}$$

$$M_t = T\sin\alpha_H + PR_H\cos\alpha_H \tag{60}$$

respectively, where α_H is the pitch angle and R_H is the radius of the helical structure. The bending moment $M_b$causes a change in curvature *k* of the coil. Therefore, the bending moment $M_b$can be expressed in terms of the curvature *k* through Eqs. (38)-(40), where *k* is substituted with $k - k^{ini}$ to take the initial curvature k^{ini} of the helix coil into account. Similarly, the torque

$M_t$causes a change in twist $k_{xy}$of the coil. Therefore, the torque $M_t$can be expressed in terms of the twist k_{xy}through Eqs. (56)-(58), wherek_{xy} is replaced by $k_{xy} - k_{xy}^{ini}$ to take the initialtwist k_{xy}^{ini} of the helix coil into account.

When only the axial load *P* is applied, Eqs. (59)-(60) can be simplified to

$$PR_H = -M_b / \sin \alpha_H \tag{61}$$

$$PR_H = M_t / \cos \alpha_H \tag{62}$$

respectively. Combining Eqs. (61) and (62) to eliminate the term PR_H gives

$$M_t \tan \alpha_H + M_b = 0 \tag{63}$$

According to the geometric relationship of a helical structure, the curvature *k* and twist k_{xy} can be expressed in terms of the pitch angle α_H and the radius R_H via

$$k = \cos^2 \alpha_H / R_H \tag{64}$$

$$k_{xy} = \cos \alpha_H \sin \alpha_H / R_H \tag{65}$$

Combining Eqs. (64) and (65) to eliminateR_H gives

$$k \tan \alpha_H - k_{xy} = 0 \tag{66}$$

Eqs. (63) and (66) are an equation set about variables$k$, k_{xy} andα_H. According to the geometric relationship, the pitch angle α_H is completely determined by the longitudinal length *h* of the helical structure if the change of the nominal length of the coil *L* during loading is negligible. For a given value of *h*, the corresponding pitch angle α_H can be found by

$$\alpha_H = \sin^{-1}(\frac{h}{h_0} \sin \alpha_{H0}) \tag{67}$$

where α_{H0} and h_0 are the initial pitch angle and longitudinal length, respectively. In an axial loading and unloading cycle, h first increases from h_0 to h_1 as the load *P* increases and then returns back to h_0 as the load is released. During this course, the pitch angleα_H can be found using Eq. (67). The curvature *k* and twistk_{xy}can be found by solving Eqs. (63) and (66) together. Finally, either Eq. (61) or (62) can be used to calculate the load *P*.

If only the torque *T* is applied, Eqs. (59) and (60) become

$$M_b = T \cos \alpha_H \tag{68}$$

$$M_t = T \sin \alpha_H \tag{69}$$

Combining Eqs. (68) and (69) to eliminate *T* yields

$$M_b \sin \alpha_H - M_t \cos \alpha_H = 0 \tag{70}$$

Again using the geometric relationship of a helical structure, there is

$$R_H = \frac{L \cos \alpha_H}{2\pi n} \tag{71}$$

where *n* is the number of turns of the helical structure. Substituting Eq. (71) into Eqs. (64) and (65) gives

$$k = 2\pi n \cos\alpha_H / L \tag{72}$$

$$k_{xy} = 2\pi n \sin\alpha_H / L \tag{73}$$

Eqs. (70), (72) and (73) are an equation set about variables$k$, k_{xy}, α_H and n. In a torsional loading and unloading cycle, the number of turns n first increases from $n_0$ton_1 as the torque *T* increases, and then returns back to $n_0$when the torque is released. For a given value of n, the corresponding curvature k, twist k_{xy} and pitch angle α_H can be found by solving Eqs. (70), (72) and (73) simultaneously. Then, use either Eq. (68) or (69) to find the torque *T*.

Finally, consider the case in which a torque *T* is applied with the longitudinal length h being fixed. This is common when a helical structure is loaded by a torque in reality. In this case, the helical structure is subjected to an applied torque *T* as well as a reaction force *P* in the axial direction. According to Eq. (67), the pitch angle α_H does not change because h is fixed. Hence, from Eqs. (71)-(73), there are

$$R_H = \frac{n_0}{n} R_{H0} \tag{74}$$

$$k = \frac{n_0}{n} k^{ini} \tag{75}$$

$$k_{xy} = \frac{n_0}{n} k_{xy}^{ini} \tag{76}$$

where n_0,R_{H0}, $k^{ini}$and k_{xy}^{ini} are respectively the initial number of turns, radius, curvature and twist of the helical structure. As the torque *T* increases and then decreases, n changes accordingly. For a given value of n, the corresponding radius R_H, curvature k and twist k_{xy}can be found through Eqs. (74)-(76). According to Eqs. (59) and (60), there are

$$T = M_b \cos\alpha_H + M_t \sin\alpha_H \tag{77}$$

$$P = \frac{-M_b \sin\alpha_H + M_t \cos\alpha_H}{R_H} \tag{78}$$

Eqs. (77) and (78) are then used to find the torque *T* and the reaction force *P*.

4. Simulation results

Mathematica was used to implement the theoretical derivation given above due to its strong ability to deal with symbolic operations. In particular, function *Piecewise* was used to define the stress distributions, function *Integrate* to implement the integrations in Eqs. (38), (40), (56) and (58), and function *FindRoot* to solve the nonlinear equations. The simulation results of the analytical model were compared to either FEA results or experimental data. The FEA results were obtained using ABAQUS/Standard, unless otherwise stated, in which the built-in user subroutine for modelling superelastic material was used, which are based on the constitutive models given by (Auricchio *et al*. 1997, Aurrichio and Sacco 1997). Table 2 lists the material constants used for the simulations in this section (Toi *et al*. 2004). Those associated with shear stress-strain relations are not independent and can be calculated according to Table 1.

As the first example, consider a straight beam subjected to a bending moment. The cross section of the beam is a 0.1 by 0.1 mm square. Fig. 5 shows the curves of the bending moment against the curvature. The solid and the dashed lines correspond to the analytical and the FEA

results, respectively. The green, red and blue lines correspond to three different magnitudes of curvatures to which the beam is bent. Note that the analytical results fit the FEA results very well for all three bending magnitudes.

Secondly, consider a straight beam with a circular cross section subjected to a pure torsion. Diameter of the section is 0.1 mm. Fig. 6 shows the curves of the torque against the twist. The solid and dashed lines correspond to the analytical and FEA results, respectively. The green, red and blue lines correspond to three different magnitudes of twist the beam is subjected to. Note that the analytical results are still comparable to the FEA results, but the agreement between the two approaches is not as good as that of the pure bending cases. According to Fig. 6, the larger the twist is, the greater the difference between the analytical and FEA results is. In general, the analytical model tends to give stiffer results than FEA does during loading.

Table 2 Material properties used in simulation

Material constant	Value	Material constant	Value
E_A	34000 (MPa)	σ_A^f	110.4 (MPa)
E_M	28500 (MPa)	ε_L	0.047
σ_M^s	427.8 (MPa)	μ	0.33
σ_M^f	542.8 (MPa)	ζ	$\sqrt{3}$
σ_A^s	210.5 (MPa)		

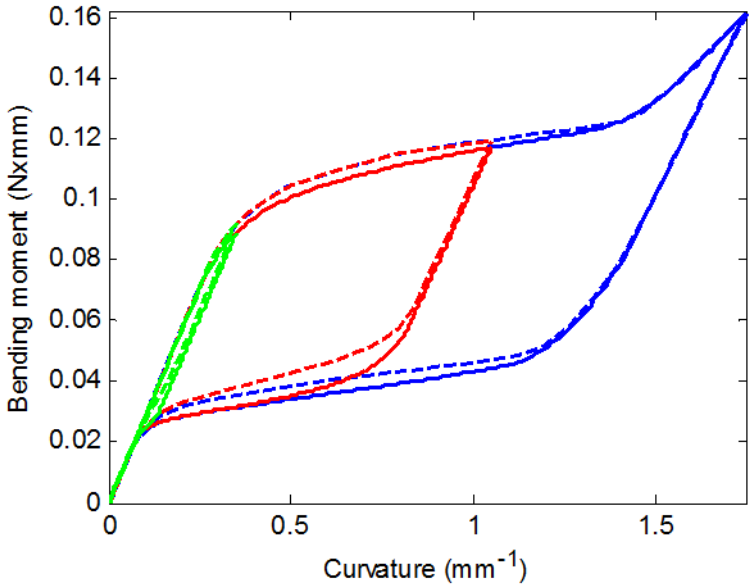

Fig. 5 Moment-curvature curves of a straight beam. The solid and dashed lines correspond to the analytical and FEM results, respectively

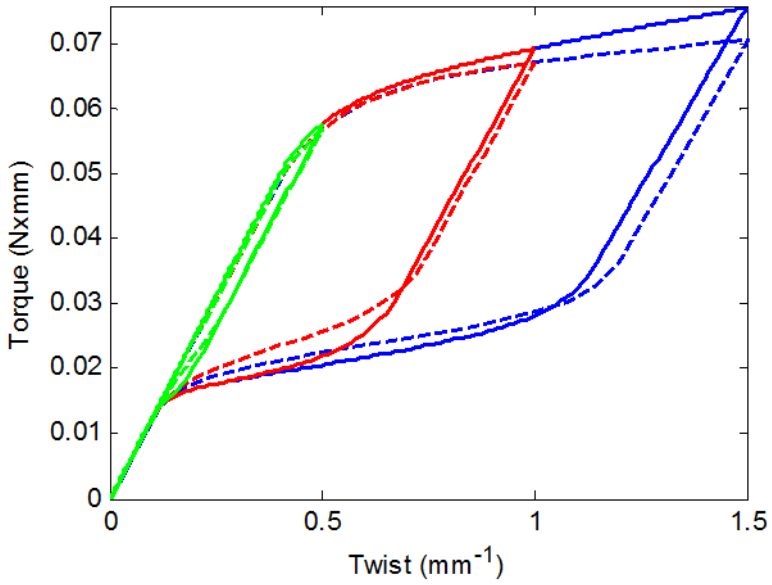

Fig. 6 Torque-twist curves of a straight beam. The solid and dashed lines correspond to the analytical and FEM results, respectively

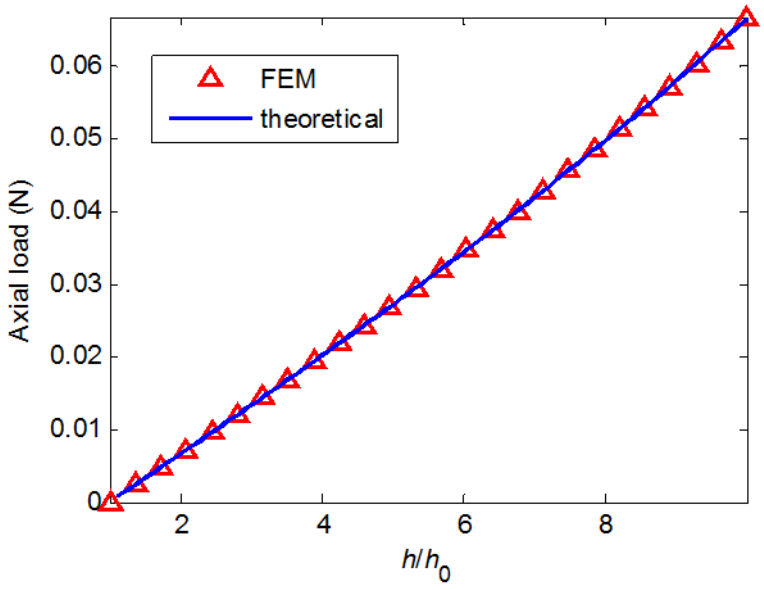

Fig. 7 Force-displacement curves of a helical structure formed by a thin coil

Consider now a helical structure formed by a thin coil with a circular cross section whose radius is 0.1 mm. The initial radiusR_{H0}, the initial pitch angle α_{H0} and the initial longitudinal length h_0 of the helical structure are 3.65 mm, 2.5° and 10mm, respectively. Two load cases, i.e., the axial load and the torsional load, are considered for this structure.

In the axial load case, the longitudinal length h of the helical structure first increases to about ten times of its original length h_0, followed by a recovery as the load is gradually released. The analytical results are compared with the results obtained by FEA. Fig. 7 shows the force-displacement curves of this load case. The horizontal axis is the ratio of the current longitudinal length to the original longitudinal length. The blue-solid lines and the red triangles correspond to the analytical results and the FEA results, respectively. Note that the analytical results are the same as the FEA results. In Fig. 7, the unloading path completely overlaps the loading path; as a result, only one path is seen. This suggests that for a helical structure formed by a thin wire, the superelastic property of SMA due to the phase transformation is not initiated even though the structure is axially loaded up to ten times of the original length.

In the torsional load case, both ends of the helical structure are fixed in the axial direction and a 360° rotation is applied to one end relative to the other end about the central axis. As a result, the helical structure is subjected to a torque as well as an axial reaction force. Fig. 8 shows the curves of the torque versus the angle of rotation. Note that the analytical model and FEA model phase transformation is initiated in this load case. Fig. 9 shows the curves of the reaction axial force versus the angle of rotation. Again, a good agreement between the analytical and FEM results is observed.

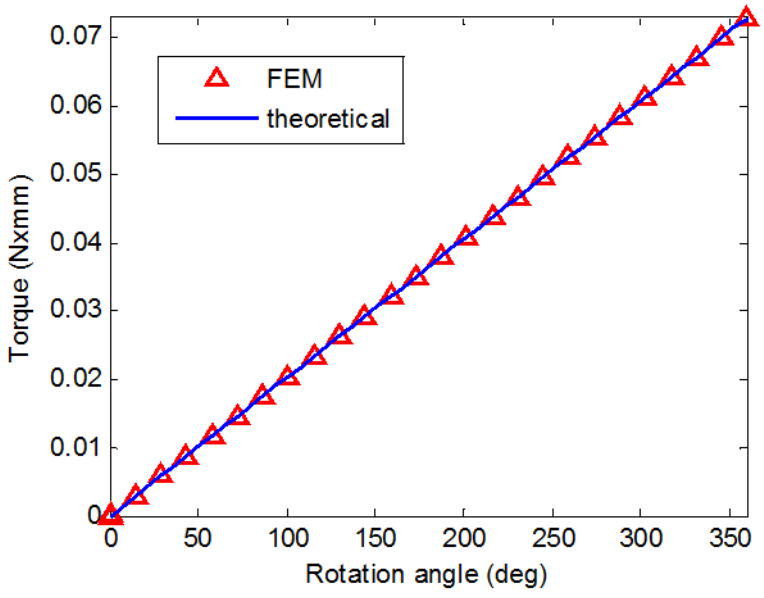

Fig. 8 Torque-angle of rotation curves of a helical structure formed by a thin coil

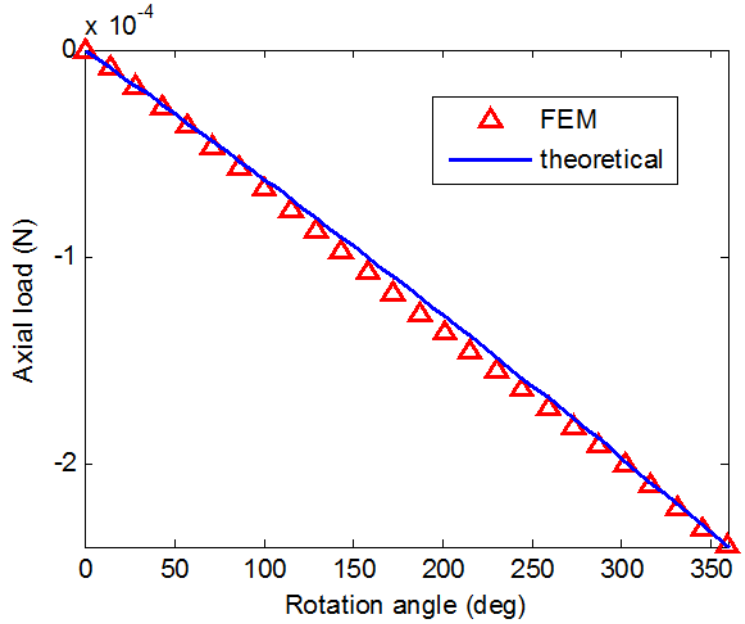

Fig. 9 Reaction force-angle of rotation curves of a helical structure formed by a thin coil

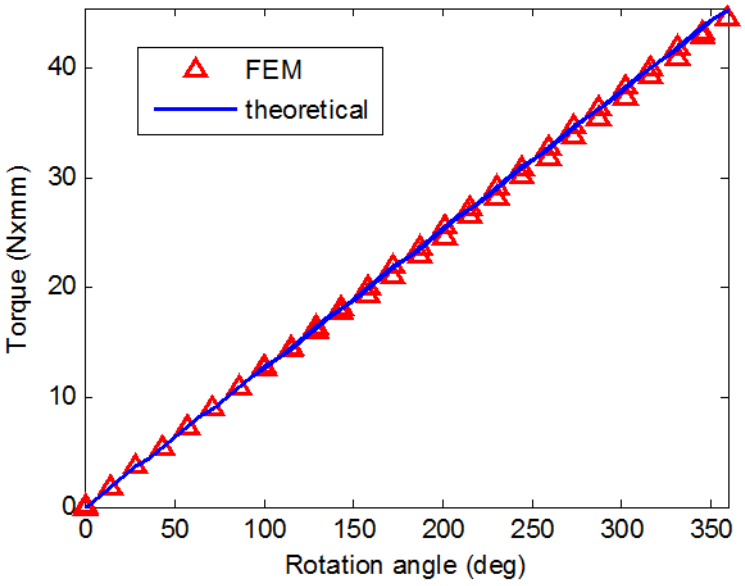

Fig. 10 Torque-angle of rotation curves of a helical structure formed by a thick coil

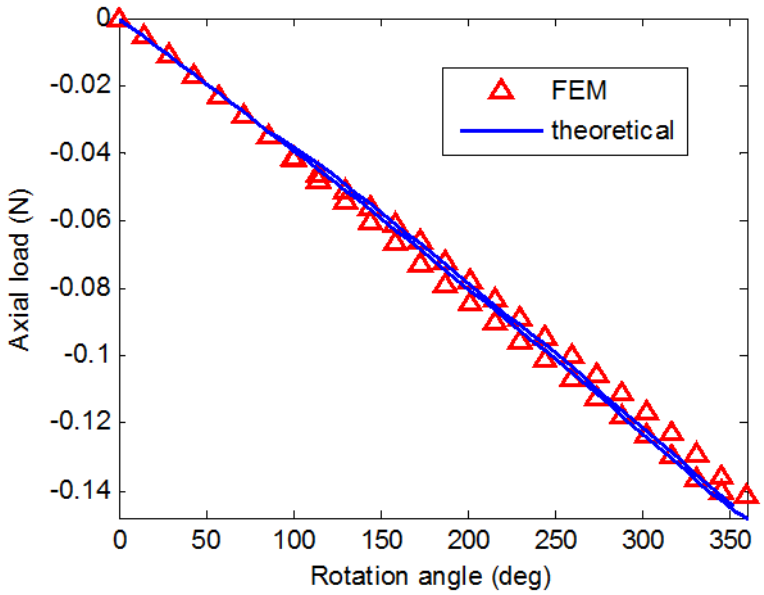

Fig. 11 Reaction force-angle of rotation curves of a helical structure formed by a thick coil

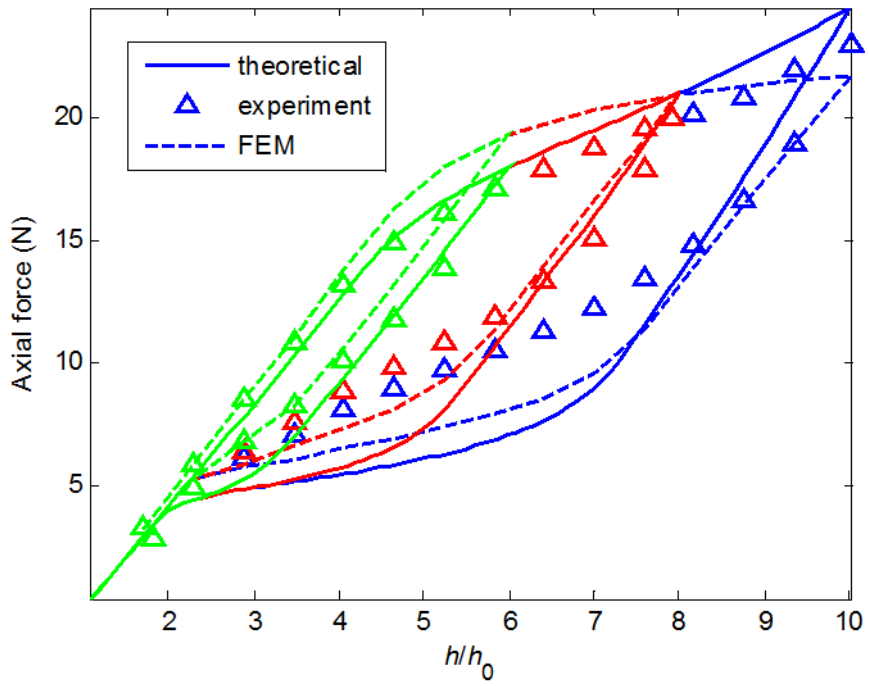

Fig. 12 Force-displacement curves of a stocky helical structure formed by a thick coil

Finally, consider a "stocky" helical structure formed by a thick coil with a circular cross section whose radius is 0.5 mm. The geometric parameters of the helical structure are the same as those for the previous example.

In the first load case for the stocky helical structure, a torsional load is applied. Again, a 360° rotation is applied to one end and both ends of the helical structure are fixed in the axial direction. Fig. 10 shows the curves of the torque versus the angle of rotation. Fig. 11 shows the curves of the axial reaction force versus the angle of rotation. Good agreements between the analytical and FEA results for both the torque and the axial reaction force can be observed. Different from the previous thin coil helical structure, both the analytical model and FEA model predicts the deviation between the loading and unloading paths, meaning that the superelastic property of the material is initiated as a result of loading. As the magnitude of torsional load is increased, the difference between the loading and unloading paths will further increase. It is found that the analytical model can calculate large hysteresis loops formed by the loading and unloading paths as the torsional load is increased. However, the FEA model encounters numerical difficulties for large torsional load.

In the second load case, an axial force is applied to the stocky helical structure. Three different load magnitudes are considered, where the longitudinal length of the helical structure is loaded to six, eight and ten times of the original length, corresponding to small, medium and large load, respectively. Instead of being compared to the FEA results obtained from ABAQUS, the analytical results are compared with the experimental data extracted from Toi *et al*. (2004). Fig. 12 shows the force-displacement curves, where the solid lines and the triangles correspond to the analytical results and the experimental data, respectively, and the green, red and blue colours correspond to the small, medium and large load magnitudes, respectively. Toi *et al*. (2004) also developed a finite element algorithm exclusively for a superelastic helical spring. The results of this analysis are also plotted in Fig. 12 in dashed lines for comparison. Note that the analytical approach predicts the force-displacement relations better than the FEA during loading and at the early stage of unloading. At the mid unloading stage, both the analytical and FEM results fail to follow the experimental data well. The discrepancy between the analytical results and the experimental data during this stage mainly owes to the assumption that the stress decreases linearly with the strain along a constant slope of E_{ξ} until the unloading plateaus is reached whereas in reality E_{ξ} gradually reduces as the stress level drops towards the unloading plateaus.At the final unloading stage, both the theoretical and FEM results are in good agreement with the experimental data again. The above comparison suggests that the analytical model is able to predict the force-displacement relationships of a stocky helical structure well and to some extent produce even better results than the FEA exclusively developed for a superelastic helical spring.

5. Conclusions

In this paper, an analytical model has been developed, which is capable of predicting the mechanical responses of superelastic SMA helical structures subject to axial and torsional loads. Three assumptions have been made to the material models, i.e., independence between the normal and shear behaviours, quantitively similarity between the normal and shear stress-strain relationships and a simplified material constitutive law. The simulation results of various structural models by using the analytical model developed in the paper are compared to the numerical results or experimental data. First, it is found that the results given by the analytical model compare well

with the FEA results. Second, when compared to the experimental data, the analytical model gives even better results than the FEA model during the loading phases. Various numerical simulations performed in this paper clearly show the capability of the analytical model to predict the large deformation of the helical structures and the non-linear behaviours in the material.

It should be noted that the theoretical approach developed in this paper has its limitations. First, it is assumed in section 2 that the superelastic normal and shear deformation behaviours are independent of each other. However, there exist experimental evidences that the superelastic normal and shear deformation behaviours are most likely to be coupled(Sun and Li 2002). The coupling leads to constitutive models for the material which is too complex to be implemented in our analytic approach. Second, the theoretical approach considers the situations in which only axial load is applied, only torsion is applied or both axial load and torsion are applied simultaneously. It does not take load histories into account, e.g. an axial load is applied and followed by an additional torsion or other loadings such as bending. Research has shown that the loading history could also change the constitutive model of an SMA sample (Berg 1995). Obviously, the material model used here is a simplification to otherwise rather intricate material behaviour, just as it was done by Atanackovic and Achenbach (1989) and Toi *et al*. (2004), without which the analytical approach would not be possible. Nevertheless, the results that we obtained compare favourably with the FEA and some experimental results which do not involve loading history. This indicates that the simplified model can still capture the main features of the SMA materials. Precisely which behaviour is more important than others in modelling SMA requires further investigation.

Acknowledgments

This work was supported by a grant from the Engineering and Physical Sciences Research Council of the UK (Grant number EP/D064732/1).

References

Arghavani, J., Auricchio, F., Naghdabadi, R., Reali, A. and Sohrabpour, S. (2010), "A 3-D phenomenological constitutive model for shape memory alloys under multiaxial loadings", *Int. J. Plasticity*, **26**(7), 976-991.

Atanackovic, T. and Achenbach, M. (1989), "Moment-curvature relations for a pseudoelastic beam", *Continuum Mech. Thermodyn.*, **1**(1), 73-80.

Aurrichio, F. and Sacco, E. (1997), "A one-dimensional model for superelastic shape-memory alloys with different elastic properties between austenite and martensite", *Int. J. Nonlinear Mech.*, **32**(6), 1101-1114.

Auricchio, F., Taylor, R.L. and Lubliner, J. (1997), "Shape-memory alloys: macromodelling and numerical simulations of the superelastic behaviour", *Comput. Method. Appl. M.*, **146**(3-4), 281-312.

Berg, B.T. (1995), "Bending of superelastic wires, part I: experimental aspects", *J. Appl. Mech. -T ASME*, **62**(2), 459-465.

Boyd, J.G. and Lagoudas, D.C. (1996), "A thermodynamical constitutive model for shape memory materials. Part I. The monolithic shape memory alloy", *Int. J. Plasticity*, **12**(6), 805-842.

Brocca, M., Brinson, L.C. and Bazant, Z.P. (2002), "Three-dimensional constitutive model for shape memory alloys based on microplane model", *J.Mech. Phys. Solids*, **50**(5), 1051-1077.

Chaudhry, Z. and Rogers C.A. (1991), "Bending and shape control of beams using SMA actuators", *J Intel. Mat. Syst. Str.*, **2**(4), 581-602.

Degeratu, S., Bizdoaca, N.G., Manolea, G., Diaconu, I., Petrisor, A. and Degeratu V. (2008), On the design of a shape memory alloy spring actuator using thermal analysis", *WSEAS Transactions on Systems*, **10**(7), 1006-1015.

He, Y.J. and Sun, Q.P. (2011), "On non-monotonic rate dependence of stress hysteresis of superelastic shape memory alloy bars", *Int. J. Solids Struct.*, **48**(11-12), 1688-1695.

Hill, B.B., Faruqi, R.M., Newman, C.E., Arko, F.R., Fogarty, T.J. and Zarins, C.K. (2004), "Successful treatment of an above-knee femoropopliteal bypass anastomotic stenosis with the aSpire covered stent", *Perspectives in Vascular Surgery and Endovascular Therapy*, **16**(3), 181-185.

Khan, E. and Srinivasan, S.M. (2011), "A new approach to the design of helical shape memory alloy spring actuators", *Smart Mater. Res.*, **2011**, 1-5.

Mansfield, E.H. (1980), "On finite inextensional deformation of a helical strip", *Int. J. Nonlinear Mech.*,**15**(6), 459-467.

Peultier, B., Ben Zineb, T. and Patoor, E. (2006), "Macroscopic constitutive law for SMA: Application to structure analysis by FEM", *Mat. Sci. Eng.: A*, **438-440**, 454-458.

Qidwai, M.A. and Lagoudas, D.C. (2000), "Numerical implementation of a shape memory alloy thermomechanical constitutive model using return mapping algorithms", *Int. J. Numer. Meth. Eng.*, **47**(6), 1123-1168.

Roguin, A., Grenadier, E., Linn, S., Markiewicz, W. and Beyar, R. (1999), "Continued expansion of the nitinol self-expanding coronary stent: angiographic analysis and 1-year clinical follow-up", *Am Heart J.*, **138**(2), 326-333.

Spinella, I. and Dragoni, E. (2010), "Analysis and design of hollow helical springs for shape memory actuators", *J. Intel. Mat. Syst. Str.*, **21**(2), 185-199.

Sun, Q. and Li, Z. (2002), "Phase transformation in superelastic NiTi polycrystalline micro-tubes under tension and torsion—from localization to homogeneous deformation", *Int. J. Solids Struct.*, **39**(13-14), 3797-3809.

Timoshenko, S. (1956), *Strength of Materials. Part 2 of 2: Advanced Theory and Problems*, D. Van Nostrand Company Inc., Princeton.

Toi, Y., Lee, J.B. and Taya, M. (2004), "Finite element analysis of superelastic, large deformation behavior of shape memory alloy helical springs", *Comput. Struct.*, **82**(20-21), 1685-1693.

vonRiesen, E.T. (2008), *Active Hyperhelical Structures*, Ph.D. Dissertation, University of Cambridge, Cambridge.

Young, W.C. (1989), *Roark's Formulas for Stress and Strain*, (6th Ed.), McGraw Hill Book Company, New York London.

Yates, S.J. and Kalamkarov, A.L. (2013), "Experimental study of helical shape memory alloy actuators: Effects of design and operating parameters on thermal transients and stroke", *Metals*, **3**(1), 123-149.

Zhou, X., You, Z. and Eaton-Evans, J. (2008), "A numerical study of a helical nitinol stent", *Proceedings of the SMST-2007 the International Conference on Shape Memory and Superelastic Technologies*, ASM International.

Zhu, S. and Zhang Y. (2007), "A thermomechanical constitutive model for superelastic SMA wire with strain-rate dependence", *Smart. Mater. Struct.*, **16**(5), 1696-1707.

CC